Three Novel Methods for Studying Complicated Diffusion Behavior Using Simple Capillary Structures

N. Yanasak[1], Q. Zhao[2], T. C-C. Hu[1], and J. Allison[1]

[1]Dept. of Radiology, Medical College of Georgia, Augusta, Georgia, United States, [2]Dept. of Physics, University of Georgia, Athens, Georgia, United States

Introduction

Diffusion tensor imaging (DTI) is an MRI-based technique used in clinical research to examine white matter structure in the brain. In spite of progress towards clinical application of this technique (1), general procedures for quality assurance (QA) and for periodic measurement of systematic bias have not been developed. In particular, the presence of noise can bias measured eigenvalues as well as anisotropy (2), suggesting the importance of monitoring anisotropy in a QA program. Phantoms with anisotropic structures have been introduced (3), although the difficulty of assembling these structures generally limits them to a prolate ("cigar"-like; e.g., capillaries) diffusive geometry. The goal of this project is to demonstrate the feasibility of and to compare the performance of three new techniques for synthesizing data with complicated diffusion characteristics, after acquiring DTI data using a simple anisotropic phantom. In this manner, the quality of data for more clinically-realistic tissue structures (e.g., oblate, or "pancake", geometry) can be inferred from phantoms that are simple to manufacture.

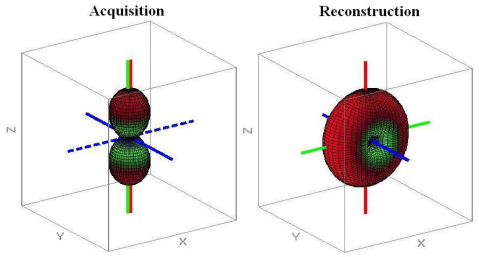

Figure 1: Using Method #1, diffusion measurements made along axes shown in color (left panel) are assumed to originate from different directions (right panel).

Methods

Theory: The first method (*Method #1*) for synthesizing complicated diffusion behavior acquires diffusion-weighted images after applying gradients along particular directions (4). The apparent diffusion coefficient (ADC) data characterizing the diffusion along these directions are assigned to a different set of gradient directions as if the gradients were applied differently. For example, ADC data that is representative of oblate structures in the plane of least-restricted diffusion (red or green axis in the "reconstruction frame" of Figure 1) must be acquired along the direction of least-restriction for a prolate structure (z-axis in the "acquisition frame" of Figure 1).

The second method (*Method #2*), applicable to the study of geometries where two white matter structures cross, requires the acquisition of two sets of DTI images. First, one applies gradients along directions in a reference frame to acquire the first set of images, then rotates to a different reference frame and applies gradients in the same directions within the new frame. For each specified direction, a pair of images will result that has identical spatial contrast except for the diffusion weighting and noise. The diffusion weighting differs according to the rotation between both reference frames, resembling two white matter structures pointing in different principal directions. Half of k-space for each pair is combined into a composite dataset after adjustment of global phase differences. Taking advantage of the conjugate nature of k-space, the composite image after Fourier transformation represents the average of diffusive behavior for each pair.

The third method (*Method #3*) acquires two identical sets of DTI images. Subtracting the two reveals the noise in a crude manner, which can be removed from diffusion-weighted signal. The raw diffusion-weighted intensity is rescaled as if diffusion within a voxel follows a different spatial distribution. Re-addition of the noise onto the raw signal biases the data as per ordinary data, although scaling may modulate the magnitude of the bias.

Data Acquisition and Analysis: A phantom was constructed, using a 1"×1"×0.4" assembly of glass capillaries arrays as previously described (3) having inner diameters of ~22 microns. All structures were filled with undoped water. The phantom was scanned in a GE Excite HDx 3.0T MRI scanner (GE Medical Systems, Milwaukee, WI), using an eight-channel phased-array head coil. Data acquired during different sessions using the prolate geometry of the capillaries were synthesized into two or three alternative diffusion geometries using each method. As a result of a lack of temperature control, the measured eigenvalues for each session are similar but not identical. The synthesized geometries, chosen to mimic tissue structure, included oblate (Methods #1 & #3 only), two prolate structures crossing at 90°, and two prolate structures crossing at 60°. The scanning protocol for each session was identical (10 slices, 5 b=0 images; b=1000 sec mm^{-2}; TR=4sec; TE=82-94msec; FOV=150mm; slice thickness=4mm; 1.5mm gap; Acq. Matrix=128×128). Data sampled along specified gradient directions were reassembled or projected along 36 directions in all cases except the 60° crossing data for Method #2 (23 gradient directions). A high-resolution FSPGR 3D image was acquired axially (155 slab positions; TE=3.9msec; TR=8.9msec; flip angle=13°; FOV=123mm; slice thickness=1mm; Acq. Matrix=256×256; NEX=0.5), to locate and verify regions of interest (ROI).

Data Analysis: Software using in-house MATLAB (Natwick, MA) scripts was used to determine the ADC values in each gradient direction and to fit tensors for prolate data; to specify appropriate gradient directions for Methods #1 & #2; and to combine, process, and synthesize data for all three methods. After data manipulation, data within all pixels of each ROI were averaged together into one spatial distribution of ADC measurements. Theoretical ADC distributions were calculated from the measured prolate eigenvalues, and RMS differences between these and actual measurements were calculated.

Results

Figure 2 shows ADC data measured and fitted to prolate distributions (top row), then projected in subsequent rows onto theoretical distributions as shown in the left column. The ADC eigenvalues for all prolate distributions were determined to be (0.6±0.2, 0.6±0.1, 2.1±0.3) ×10^{-3} mm^2 sec^{-1}. In general, correspondence between the expected and measured distributions is qualitatively good. RMS differences between the theoretical and measured ADC values range from ~5-19×10^{-5} mm^2 sec^{-1} for Method #1, ~20-55×10^{-5} mm^2 sec^{-1} for Method #2, and ~2-5×10^{-5} mm^2 sec^{-1} for Method #3. In Figure 2, some data for Method #2 are plotted beneath the grey theoretical distribution surface due to larger RMS values.

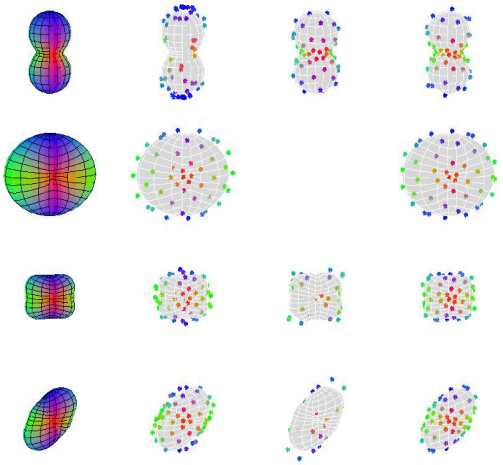

Figure 2: Comparison of the distribution of ADC values, using methods to generate oblate (row 2), 90° crossing prolate (row 3), and 60° crossing prolate (row 4) geometry from individual prolate data (row 1). Column 1: Theoretical distributions. Columns 2-4: Methods #1-3.

Discussion

These results demonstrate that these three techniques can produce ADC distributions representative of crossing white matter tissues, employing a simple capillary phantom. Potentially, other complex structures could be produced, including those with three or more crossing tensor components. Further investigation is warranted to characterize fully the noise behavior of these synthesized data sets, for validating their use as a proxy for complicated, restricted diffusive behavior. Surprisingly, data for Method #2 deviates more from expectation than the other methods, possibly due to recombination errors in k-space processing or due to the methodology itself.

References

1) Hagmann P., et al. 2003. Neuroimage 19: 545-54.
2) Basser PJ, et al. 2000. Magn. Reson. Med. 44: 41-50.
3) Yanasak NE, et al. 2006 Magn. Reson. Imag. 24: 1349-61.
4) Yanasak NE, et al. 2007. Med. Phys. 34 : 2349.